Serially Concatenated Schemes for Single Sideband Continuous Phase Modulation

Abhishek Kumar, Haifa Fares, Yves Louet

IEEE Open Journal of the Communications Society

Received XX Month, XXXX; revised XX Month, XXXX; accepted XX Month, XXXX; Date of publication XX Month, XXXX; date of current version XX Month, XXXX.

Digital Object Identifier 10.1109/OJCOMS.2022.1234567

Serially Concatenated Schemes for Single Sideband Continuous Phase Modulation

Abhishek Kumar*, Haïfa Farès*, and Yves Louët*

[1]IETR - UMR CNRS 6164, CentraleSupélec, Université Paris Saclay, Rennes Campus, avenue de la Boulaie - CS 47601 35576 CESSON-SEVIGNE Cedex, France

CORRESPONDING AUTHOR: Abhishek Kumar (e-mail: abhishek.kumar@@centralesupelec.fr).

ABSTRACT This paper investigates serially concatenated (SC) and interleaved transmission schemes for a new class of continuous phase modulation (CPM), which has the property being a single sideband (SSB). This new CPM is commonly called Single Side-Band Frequency Shift Keying (SSB-FSK). Due to the ample space of SSB-FSK parameters, finding good serially concatenated schemes using SSB-FSK with desired spectral and energy efficiencies as well as reasonable complexity, is challenging. We present a systematic, simulation-based extrinsic information transfer (EXIT) chart approach to evaluate this multi-objective problem (improve spectral and energy efficiencies and reduce complexity) and subsequently design a competitive serially concatenated SSB-FSK based scheme. We show that iterative decoding of SC schemes using SSB-FSK (SC-SSB-FSK) provides close to optimal performance. Furthermore, the bit error rate (BER) of SC-SSB-FSK is compared to that using raised cosine (RC) based CPM signals. It has been shown that the proposed technique outperforms the state-of-the-art serially concatenated systems.

INDEX TERMS Serially concatenated schemes, SSB signal, CPM waveform, power-limited applications, 6G.

I. Introduction

CONSTANT envelope continuous phase modulation (CPM) schemes are extremely important in peak power-limited communication applications such as satellite transmission systems. Recently, a new class of CPM has been proposed in [1]. The original feature of this CPM waveform is generating a single sideband (SSB) signal *directly* by using a generic frequency pulse with a *Lorentzian* shape. The Lorentzian pulse has a specific shape addressing fundamental quantum physics, particularly the on-demand injection of a single electron in the quantum conductor [2] and [3] with the demonstration of a new quasi-particle called ”Leviton”. By extrapolating the quantum energy spectrum that became one-sided when using levitonic elementary pulses to the domain of the frequency spectrum for digital communications [1], [4], we achieve the first application of Levitonics to digital transmission based on CPM, known as single sideband frequency shift keying (SSB-FSK) signal. The study conducted in [5] reconsiders the approach of pulse amplitude modulation (PAM) decomposition and adapts it to the singularities of SSB-FSK. Consequently, the authors succeeded to design a simplified receiver for generic binary SSB-FSK based on Kaleh’s suboptimal receiver [6]. In [7], authors reported a complete study of the SSB-FSK performance, regarding error probability (energy efficiency), spectral efficiency, complexity, and SSB property depending on many tuning parameters: parameters usually considered in CPM (modulation index, pulse length, modulation order) and another one specific to the use of the Lorentzian pulse, which is the pulse width. The results in terms of optimal performance of the SSB-FSK scheme are presented as Pareto optimum frontiers when energy-bandwidth interplay is considered. When adding receiver complexity as a third objective function, some configurations with interesting tradeoffs have been retained. It is worth noting that special interest has been given to one configuration with an integer modulation index since it is combining good performance and synchronization advantage. For instance, this integer modulation index generates deterministic spikes on the resulting spectrum, which can be exploited for synchronization without the need of designing a specific preamble for this purpose.

Even if [7] gives good guidelines for designing systems using SSB-FSK, the study remains incomplete since no

This work is licensed under a Creative Commons Attribution 4.0 License. For more information, see https://creativecommons.org/licenses/by/4.0/

forward error correcting (FEC) channel code was considered so far. The FEC concatenated CPM is commonly called a serially concatenated code (SCC). Different schemes for bit-interleaved coded CPM, SC-CPM, are presented in [8], [9], [10], where SC-CPM showed a significant improvement compared to the convolution coded system. With the inherent coding property in CPM, SC-CPM, that is, coded and interleaved CPM with iterative decoding was proposed [8] and showed a significant improvement. Hence, The major aim of this paper is then to evaluate the potential of this new waveform in the presence of channel coding. A particular interest is intentionally granted to the concatenated implementation able to achieve iterative decoding gain at the receiver side. On another side, as considering non-iterative transmission made implementation easier, it is naturally important to add comparisons with non-iterative implementations. The detailed contributions of the manuscript are listed below:

1) We proposed maximum *a Posteriori* (MAP) detector to perform Soft-Input Soft-Output (SISO) decoding of the SSB-FSK modulated signal. BCJR algorithm is employed to implement the MAP detector. The novel transition matrix for the BCJR algorithm is obtained based on the PAM decomposition of the SSB-FSK modulated signal, taking into account all singularities of this waveform.
2) The performance of the MAP detector based on the BCJR algorithm has been simulated. It is observed that the bit error rate (BER) curves of the MAP detector asymptotically reach the performance analysis bounds.
3) We implemented the serially concatenated scheme using SSB-FSK (SC-SSB-FSK) with a conventional convolutional encoder (CC) and its iterative decoding. The SISO decoding of CPM (contribution 1) as well as that of CC, are used for the elementary decoders needed inside the whole iterative decoder. A detailed algorithm for the iterative decoding of the SC-SSB-FSK signal is presented.
4) An extensive extrinsic information transfer (EXIT)-chart analysis is carried out to analyze the convergence abilities of the iterative decoder. The Pareto frontier parameters of SSB-FSK reported in [7] are used to analyze the EXIT chart performance.
5) We analyzed the iterative decoder performance in the presence of adjacent channel interference (ACI). The EXIT-based analysis is carried out to present the Pareto frontier in the presence of ACI limiting the spectral efficiency. The optimization result is given in terms of a minimal number of iterations needed in order to converge under given environment conditions (assuming a fixed amount of ACI). In this part, we confirmed the intuition that SC-SSB-FSK will perform better since they are generating one-sided spectrum being less sensitive to the interference coming from ACI, compared to familiar CPM systems generating double-sided spectrum.
6) We illustrated BER performance of the proposed iterative decoder performed on the retained SC-SSB-FSK configuration, resulting from the EXIT-based analysis. The BER performance of SC-SSB-FSK is compared to that resulting from using the raised cosine (RC) CPM signal, and it has been shown that the proposed technique outperforms state-of-the-art serially concatenated CPM-based systems.

The rest of the paper is organized as follows: In Section II, we perform the preliminaries required study of the SSB-FSK signal, and we present an SC system model for the SSB-FSK signal. Section III presents MAP demodulation of the SSB-FSK signal with a performance analysis of the demodulator. The detailed study of the SC scheme of SSB-FSK and its iterative decoding algorithm based on MAP demodulation is developed in Section IV. SSB-FSK parameters analysis based on the EXIT chart and its optimization in the presence of ACI is presented in Section V. In Section VI, we showed that the iterative decoding of SC-SSB-FSK could reach an optimum bit error rate (BER) performance and outperform the state-of-the-art SC scheme of RC CPM signal. Finally, conclusions are made in Section VII.

II. Preliminaries

In this section, we recall all the needed materials to carry out the performance evaluation of SSB-FSK in the presence of an FEC code concatenated in an interleaved manner in order to perform iterative decoding at the receiver. We get through the EXIT-chart tool to quantify the contribution of SSB-FSK in concatenated schemes compared to conventional CPM forms. To do so, we need to develop the MAP SISO decoder of the SSB-FSK. This decoder is developed based on the definition of the PAM decomposition of the SSB-FSK scheme. Consequently, in this section, we particularly recall both the signal model highlighting its singularities and the PAM decomposition of the SSB-FSK signal for integer and non-integer modulation indices. Both types of modulation indices are discussed throughout the paper in order to be the most generic possible and to consider all interesting configurations, as long as we no longer see SSB-FSK as a single waveform but a class of CPM waveforms.

A. SSB-FSK Signal Model

The new CPM, SSB-FSK, uses a generic phase derivative pulse $d\phi/dt$ with Lorentzian shape and 2π phase increment. The Lorentzian pulse is a specific shape that addresses fundamental quantum physics, particularly the on-demand injection of a single electron in a quantum conductor. Following a theoretical proposal by Levitov et al. [11], a short voltage pulse $V(t)$ is applied to a contact of the conductor, resulting in a current pulse $I(t) = 2e^2V(t)/h_0$ (e is the electron charge and h_0 is the Planck constant). A single electron is injected from the contact into the conductor by tuning the pulse amplitude and duration so that the net charge $Q = \int I(t)dt = e$. However, the voltage pulse

perturbs all the electrons of the conductor, creating unwanted excitations. Levitov et al. in [11] showed that if $V(t)$ has a Lorentzian shape (and only this shape), a pure single-electron state is created: A Leviton. The experimental demonstration of Levitons and their exploitation is given in [2], [3], thus laying the foundation for quantum Levitonics. When $V(t)$ is a Lorentzian pulse, the electron energy distribution (equivalently frequency spectrum) becomes SSB.

The complex envelope carrying the binary information of the SSB-FSK signal is defined as

$$s(t,a) = \sqrt{E_s/T_s}\exp\{j\phi(t,a)\} \tag{1}$$

$$\phi(t,a) = 2\pi\tilde{h}\sum_{i=-\infty}^{+\infty} a_i\phi_0(t-iT_s) \tag{2}$$

where E_s is the signal energy per symbol, T_s is the symbol interval, $\tilde{h} = 2h$, where h is the modulation index used to ensure a 2π phase increment, and $a = \{a_i \in [0,1]\}$ denotes the information binary sequence (no antipodal coding is perfromed). The information symbols a_i are assumed to be independent and identically distributed (i.i.d). $\phi_0(t)$ is a Levitonic phase shift function and is given by [2]:

$$\phi_0(t) = \begin{cases} 0 & t < 0 \\ 1/4\pi\int_{-\infty}^{t} g(\tau)d\tau, & 0 \le t \le LT_s \\ 1/2 & t \ge LT_s \end{cases} \tag{3}$$

here, $g(t)$ is a truncated Lorentzian pulse of duration $LT_s \geq 1$ (Partial response) symbol duration, defined as

$$g(t) = \frac{d\varphi_0(t)}{dt} = \mu\frac{2w^2}{t^2+w^2},\ t \in [-LT_s/2, LT_s/2] \tag{4}$$

leading to $\varphi_0(t)$ a Levitonic phase-shift function, given by

$$\varphi_0(t) = 2\mu\arctan\left(\frac{t}{w}\right). \tag{5}$$

The variable w is the pulse width, μ is the correcting factor introduced to keep an exact 2π phase increment after frequency pulse truncation, and is defined as

$$\mu = \frac{2\pi}{\int_{-LT_s/2}^{LT_s/2}\frac{2w^2}{t^2+w^2}dt} = \frac{\pi}{2\arctan\left(\frac{LT_s}{2w}\right)} \tag{6}$$

The derivative of the total phase $\phi(t,a)$ is then a sum of overlapping Lorentzians $\frac{2\mu w^2}{(t-kT_s)^2+w^2}$, centered on kT_s weighted by the symbols a_i and truncated to the length LT_s. For the non-truncated Lorentzian pulse $(L=\infty)$, $\mu = 1$ (no correction is required).

1) Spectrum Analysis:

The Fourier transform of the complex signal $x(t) = e^{-j\phi(t)}$ is defined by

$$X(f) = \int_{-\infty}^{\infty} e^{-j\phi(t)}e^{-j2\pi ft}dt \tag{7}$$

The necessary condition to obtain a single side-band spectrum is to have a finite value for $f > 0$ and a zero value for $f < 0$. Accordingly, $x(t)$ should at least have one pole in the upper and no poles in the lower complex plane. The simplest mathematical form of $x(t)$ respecting these conditions is given by [12]:

$$x(t) = e^{-j\phi(t)} = \frac{t-t_0+jw_0}{t-t_0-jw_0} \tag{8}$$

where the pole has been arbitrarily chosen at $t = t_0 + jw_0$, with w_0 is the pulse width at a pulse time t_0. As a result, the general levitonic phase term $\phi(t) = \varphi(t_0) = 2\arctan\left(\frac{t-t_0}{w_0}\right)$ is formed, and the elementary frequency pulse is given by its derivative

$$g(t) = \frac{2w_0}{(t-t_0)^2+w_0^2}. \tag{9}$$

This results on the Fourier transform $X(f) = e^{-4\pi w_0 f}$ for $f > 0$ and zero otherwise. The extension of this idea is to add more poles only in the upper complex plane, allowing $X(f)$ to keep the original SSB property. Precisely, this extension entails producing more complex phases, which are the sum of N elementary phases $\phi_i(t)$ of type $\varphi_0(t)$ that occur at time t_i and width w_i, $(wi > 0)$. As a result, the general form of $x(t)$ is

$$x(t) = e^{-j\phi(t)} = \prod_{i=0}^{N-1}\frac{t-t_i+jw_i}{t-t_i-jw_i} \tag{10}$$

and the general form of the phase shift function $\phi(t)$ is

$$\phi(t) = \sum_{i=0}^{N-1} h_i\varphi(t) \tag{11}$$

Where h_i are integers with the same sign. If $h_i > 0\ \forall\ i$, $X(f) = 0;\quad f < 0$, and similar if $h_i < 0\ \forall\ i, X(f) = 0;\quad f > 0$. This explains why no antipodal coding is used on the modulated information bits.

B. PAM Decomposition of SSB-FSK

In this subsection, we perform the PAM Decomposition of CPM signals with integer/non-integer modulation indices. To do so, we had to rewrite the SSB-FSK signal to retrieve the same initial assumptions considered in the derivations presented in [13] and [14]. Hence, the signal $s(t,a)$ given in (2) is strictly equivalent to

$$\begin{aligned} s(t,a) &= e^{j2\pi\tilde{h}}\sum_{i=-\infty}^{+\infty} a_i\phi_0(t-iT_s) \\ &= \underbrace{e^{j2\pi h}\sum_i \tilde{a}_i\phi_0(t-iT_s)}_{s_1(t,\tilde{a})}\quad\underbrace{e^{j2\pi h}\sum_i \phi_0(t-iT_s)}_{s_2(t)} \end{aligned} \tag{12}$$

where $\tilde{a}_i = 2a_i - 1 \in [-1,1]$. According to the above equation, the baseband SSB-FSK signal $s(t,a)$ could be viewed as a product of two independent signals $s_1(t,\tilde{a})$ and $s_2(t)$. Here, $s_1(t,\tilde{a})$ is dependent on the antipodal coded information symbols $\tilde{a}$, and $s_2(t)$ is a deterministic signal that does not carry any information.

1) PAM decomposition of SSB-FSK with non-integer modulation index

For non-integer modulation indices, we followed the derivations given by Laurent in [14], where $s_1(t,\tilde{a})$ can be reformulated as

$$s_1(t,\tilde{a}) = \sum_{k=0}^{Q-1}\sum_{n} b_{k,n}c_k(t-nT_s) \tag{13}$$

where $Q = 2^{L-1}$ is the number of pulses required for an exact signal representation. The PAM pulse $c_k(t)$ is defined as:

$$c_k(t) = \prod_{i=0}^{L-1} u(t+iT_s+\beta_{k,i}LT_s), \qquad 0 \le t \le D_kT_s. \tag{14}$$

The function $u(t)$ is given by

$$u(t) = \begin{cases} sin(2\pi h\phi_0(t)) & 0 \le t \le LT_s \\ u(2LT_s - t), & LT_s \le t \le 2LT_s \\ 0 & \text{otherwise} \end{cases} \tag{15}$$

Note that the parameters $\beta_{k,i}$ can only take the values 0 or 1 and are obtained from the equality

$$k = \sum_{i=1}^{L-1} 2^{i-1}\beta_{k,i}, \tag{16}$$

Additionally, D_k is the k^{th} pulse duration, defined as

$$D_k = \min_i L(2-\beta_{k,i}) - i, \qquad 0 \le i \le L-1 \tag{17}$$

Finally, the mapping between the pseudo-symbols and the information data a_i follows the expression

$$b_{k,n} = \exp\left\{ jh\pi \left[\sum_{m=-\infty}^{n} \tilde{a}_m - \sum_{i=0}^{L-1} \tilde{\alpha}_{n-i}\beta_{k,i} \right] \right\} \tag{18}$$

2) PAM decomposition of SSB-FSK with integer modulation index

For integer modulation indices, we follow the derivations given by Huang et al. [13], stating that the signal $s_1(t,\tilde{a})$ can be represented as

$$s_1(t,\tilde{a}) = \sum_{n} J^n \left[h_0(t-nT) + \sum_{k=1}^{2^{L-1}} B_{k,n}h_k(t-nT) \right] \tag{19}$$

where $J = cos(h\pi)$. The PAM pulses $h_0(t)$ and $h_k(t)$ are defined as

$$\begin{aligned} h_0(t) &= \prod_{i=-L+1}^{0} \cos\phi_0(t-iT), \quad 0 \le t \le T \\ h_k(t) &= \prod_{i=1}^{L-1} \cos\phi_0(t-iT) \prod_{i=0}^{L-1} [(1-\beta_{k,i}) \\ &\quad \cos\phi_0(t+iT) + \beta_{k,i}\sin\phi_0(t+iT)], \\ &\quad 0 \le t \le L_kT \end{aligned} \tag{20}$$

The parameter $\beta_{k,i}$ is determined by the equality

$$2k-1 = \sum_{i=0}^{L-1} 2^i\beta_{k,i} \quad 1 \le k \le 2^{L-1} \tag{21}$$

Additionally, L_k is the k^{th} pulse duration, defined as

$$L_k = L - \max_{\beta_{k,i}\neq 0} i. \tag{22}$$

Finally, the mapping follows the expression

$$B_{k,n} = \prod_{i=0}^{L-1} (1-\beta_{k,i} + \beta_{k,i}j\tilde{\alpha}_{n-i}) \tag{23}$$

The maximum number of PAM pulses N is given by:

$$N = \begin{cases} Q-1, & (\text{non-integer } h), \\ 2^{L-1}, & (\text{integer } h) \end{cases} \tag{24}$$

The number of states for the PAM-based decomposition

$$N_s' = pM^{L'-1} \tag{25}$$

where

$$\begin{aligned} L' &= L+1-l_{min}, \\ l_{min} &= \min_k l_k, \qquad 0 \le k \le N_0 \end{aligned} \tag{26}$$

C. Serially Concatenated System

A schematic of an SC-SSB-FSK system is shown in Fig. 1. It consists of a conventional binary CC, a symbol interleaver, an SSB-FSK modulator, and an iterative decoder able to decode this serially concatenated code [8], [10], [15]. Based on the general definition of the SSB-FSK CPM family, the modulation index is given by $h = k/p$, where k and p are relatively prime positive integers. The received CPM signals have experienced an additive Gaussian white noise (AWGN) channel with single-sided power spectral density N_0. The decoder consists of two SISO decoders D_1 and D_2, matched to the outer code and the CPM modulator, respectively. These two SISO modules perform MAP detection. Iterations are performed on the extrinsic log-likelihood ratio between CPM and the channel encoder. The output from the CPM MAP (interleaved to be input to the outer code) is extrinsic information for the output symbol of the outer code since the extrinsic input values for the outer MAP are obtained directly from deinterleaving the CPM inner MAP output.

The equivalent baseband received signal, denoted by $r(t)$, is defined as

$$r(t) = s(t,\mathbf{c}_1^k) + n(t), \tag{27}$$

where $n(t)$ is a complex baseband AWGN with zero mean and power spectral density N_0. $\mathbf{c}_1^k$ is the interleaved output of CC, which is given by $\mathbf{c}_1^k = [u_k, p_k]$, the codeword produced by the outer code whose input is the information sequence $\mathbf{u} = [u_1, u_2, \ldots, u_K]$. The Maximum Likelihood sequence estimation (MLSE) aims at maximizing the scalar product between $r(t)$ and all possible realizations of $s(t,c_1^k)$.

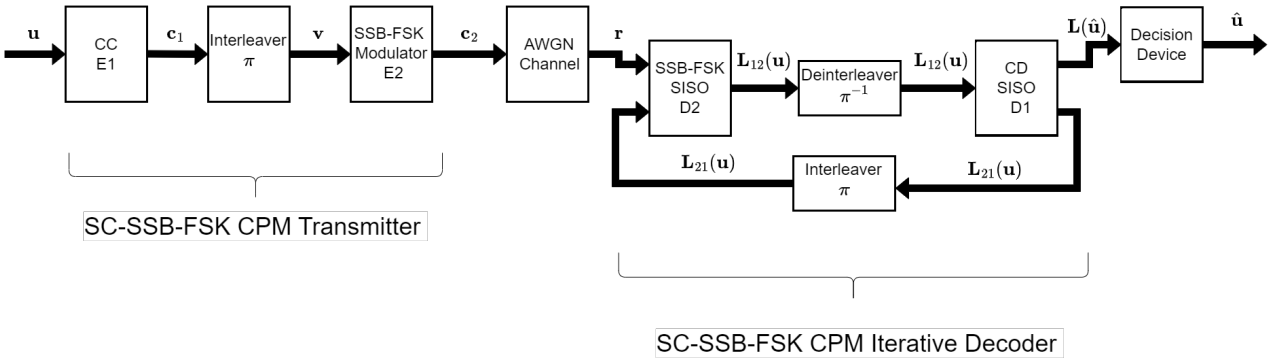

FIGURE 1. **SC-SSB-FSK transmitter and its iterative decoder block diagram**

Assuming K transmitted symbols, the MLSE estimation of the information symbols $u_0, u_1, ..., u_{K-1}$ is given by

$$(\hat{u}_0, \hat{u}_1, \dots \hat{u}_{K-1}) = arg \max_{u \in \mathcal{M}^K} \mathcal{R}\left[\int_0^{NT} r(t) S^*(t, c_1^k) dt\right]. \quad (28)$$

where $\mathcal{R}(X)$ denotes the real part of X and $\mathcal{M}$ is the constellation alphabet.

III. MAP demodulator of SSB-FSK signal

The MAP detection is widely used in turbo decoders, turbo demodulators, and turbo equalizers where SISO detectors are required. Hereafter, a BCJR based MAP demodulator is derived in order to be able to consider SSB-FSK for concatenated and interleaved schemes. In this section, we present the BCJR implementation of MAP demodulation of SSB-FSK presents some differences with common CPM waveforms.

The MAP decoding criterion for the received signal of (2) is given by,

$$\hat{a}_i = \text{argmax} \quad (\tilde{a}_i) \left[P(\tilde{a}_i|\mathbf{r})\right] \quad (29)$$

where $P(\tilde{a}_i|\mathbf{r})$ is the *a posteriori* probability (APP) of the information bit $\tilde{a}_i$ given the received word $\mathbf{r}$, $\tilde{a}_i \in \{+1, -1\}$ over $a_i \in \{0, 1\}$. Given $\tilde{a}_i$, the bit-wise MAP rule simplifies to

$$\hat{a}_i = \text{sign}\left[L(\tilde{a}_i)\right] \quad (30)$$

Where $L(\tilde{a}_i)$ is the logarithmic APP (log-APP) ratio defined as

$$L(\tilde{a}_i) \triangleq \log\left[\frac{P(\tilde{a}_i = +1|\mathbf{r})}{P(\tilde{a}_i = -1|\mathbf{r})}\right] \quad (31)$$

$$= \log\left[\sum_{U^+} \exp\left(\alpha_{i-1}(s') + \gamma_i(s', s) + \beta_i(s)\right)\right] - \log\left[\sum_{U^+} \exp\left(\alpha_{i-1}(s') + \gamma_i(s', s) + \beta_i(s)\right)\right] \quad (32)$$

Where s is the i^{th} encoder state, and s' is the $(i-1)^{th}$ encoder state. U^+ is the set of pairs (s', s) for the state transitions $s' \rightarrow s$, which corresponds to the event $a_i = +1$, and U^- is similarly defined for the event $a_i = -1$. The probability $\gamma_i(s', s)$ is the state transition probability, the probability $\alpha_i(s)$ is computed in a "forward recursion" for the sum of all possible encoder states, and the probability $\beta_i(s)$ is computed in a "backward recursion" for the sum of all possible encoder states. Hence, to apply antipodal coding keeping the SSB property, the equivalent expression of SSB-FSK given in (12) is considered. Next, by using max-log approximation given in Chapter 4 of [16], (32) is further reduced to,

$$L(\hat{a}_i) = \max_{U^+}{}^{*} \left[\alpha_{i-1}(s') + \gamma_i(s', s) + \beta_i(s)\right] - \max_{U^-}{}^{*} \left[\alpha_{i-1}(s') + \gamma_i(s', s) + \beta_i(s)\right] \quad (33)$$

Here, $\alpha_i(s) = \max_{s'}^{*} \left[\alpha_{i-1}(s') + \gamma_i(s', s)\right]$, and $\beta_{i-1}(s') = \max_{s}^{*} \left[\beta_i(s') + \gamma_i(s', s)\right]$. The transition probability γ and the recursion probabilities α and β are calculated using a Viterbi-like structure. The PAM decomposition for $s_1(t, a)$ is used to obtain the Viterbi-like structure for the SSB-FSK signal, which is used to calculate the recursion and transition probabilities of all possible states and is obtained using eqs. (13) and (19) for h non-integer and integer, respectively. Here, we use the PAM decomposition of the received SSB FSK signal correlating with all possible cases to find the γ values, as the SSB-FSK does not support the antipodal coding scheme. In the normal scenario, we directly correlate the received signal to all possible states. The branch metrics of the proposed MAP SISO detector are derived based on this PAM decomposition, itself based on the reformulation of the signal model in order to integrate an equivalent signal model using anti-podal coding. This difference is essential to achieve the potential of this new waveform. Without adapting this SISO detector to this particular property, the original MAP SISO detector does not perform well. The

initial condition for α and β probabilities are defined as:

$$\alpha_0(s) = \begin{cases} 0, & s = 0, \\ -\infty & s \neq 0 \end{cases} \tag{34}$$

and,

$$\beta_N(s) = \begin{cases} 0, & s = 0, \\ -\infty & s \neq 0 \end{cases} \tag{35}$$

The pseudo-code of the MAP detection of SSB-FSK signal is presented in Algorithm 1 in Appendix A.

In the following, we present simulation results of BCJR-based MAP decoder for two case studies for SSB-FSK schemes:

- Use case (A): $L = 5,\ h = 1,\ M = 2$ and $w = 0.8$,
- Use case (B): $L = 9,\ h = 1,\ M = 2$, and $w = 0.8$.

The parameters selection for these schemes was conducted in [5] using the Pareto optimum multi-objective optimization. Besides, in [17, Ch. 9, Sec. 1] and [18], the authors show an advantage of using integer modulation index h for synchronization. Nevertheless, CPM schemes with integer h are usually avoided due to their weak performance [17], which is not the case of SSB-FSK CPM family. Therefore, both the study cases in this part are considering integer modulation index, particularly $h = 1$, since integer modulation indices $h > 1$ show poor normalized bandwidth occupancy. It is worth noting that integer modulation indices present a valuable advantage in terms of complexity leading to less phase states, since no cumulative phase has to be considered. However, more use cases (considering non-integer modulation indices) will be considered in the EXIT-Chart analysis part in order to be more generic in designing SC-SSB-FSK schemes.

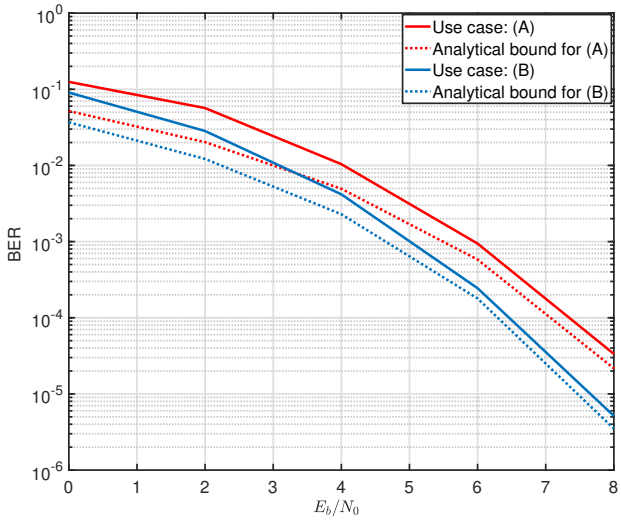

FIGURE 2. BER plots of BCJR detector of SSB-FSK signal for both the use cases (A) and (B).

The Fig. 2 presents the BER plots for the BCJR detection of the SSB-FSK signal for both use cases (A) and (B). These

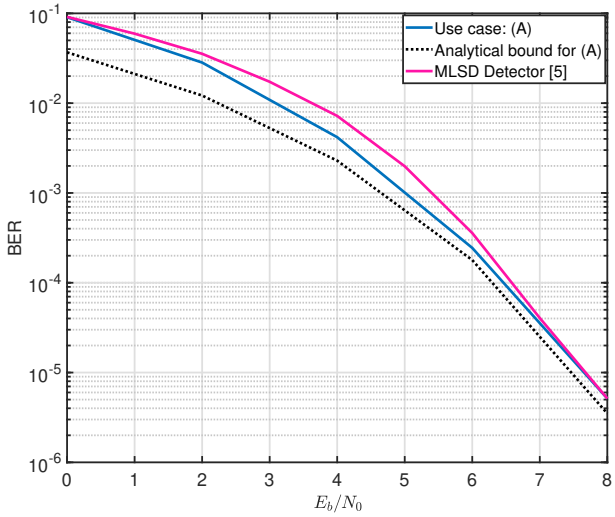

FIGURE 3. BER plots comparison of BCJR detector with VA-based MLSD for SSB-FSK signal for the use case (B).

BER curves are plotted along with the lower bound for the same configurations of the SSB-FSK schemes. It is evident that BCJR-based detector asymptotically reaches the bound for both configurations. The analytical bonds are plotted based on the minimum squared Euclidean distance d^2_{min} obtained from the aforementioned Pareto frontiers which are 2.66, and 3.27 for use cases (A) and (B), respectively.

In Fig. 3, a BER comparison of BCJR and VA-based MLSD of SSB-FSK modulated signal is presented. This illustration clearly depicts that the BCJR detection outperforms the VA-based MLSD in the mid-range of the $E_b/N_0 =$ 3 to 6 dB. However, both techniques asymptotically reach the bound, showing the effectiveness of the BCJR detection of SSB-FSK modulated signal.

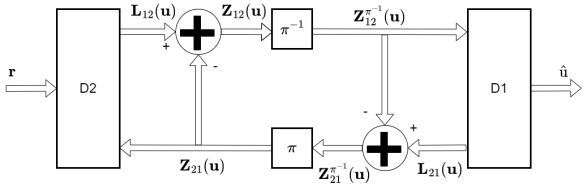

FIGURE 4. Detail Iterative Decoder Structure

IV. The SC-SSB-FSK Iterative Decoder

This section presents the iterative decoder for an SC-SSB-FSK consisting of one 1/2-rate recursive systematic convolutional (RSC) encoder with generator matrix $(G = [1, 5/7])$ transfer function, a pseudo-random interleaved, and an SSB-FSK modulator. We assume no puncturing. A block diagram of the SC-SSB-FSK iterative decoder with component SISO decoders is presented in Figure 4. As mentioned before,

$\mathbf{c}_1^k = [u_k, p_k]$ denotes the codeword produced by the convolutional encoder E1 whose input is the information sequence $\mathbf{u} = [u_1, u_2, \ldots, u_K]$. We likely denote by $\mathbf{c}_2^k$ the codeword produced by the SSB-FSK modulator (E2) whose input is the interleaved version of $\mathbf{c}_1^k$.

The iterative SC-SSB-FSK decoder in Fig. 4 employs two SISO decoding modules. These SISO decoders share extrinsic information on both codewords $\mathbf{c}_k^1$ and $\mathbf{c}_k^2$ under the assumption of being known at both encoders E1 and E2 (CC and SSB-FSK modulator). A consequence is that the SISO decoder D1 must provide likelihood information on E1 output bits, whereas SISO decoder D2 produces likelihood information on E2 input bits, as indicated in Figure 4. Furthermore, because LLRs must be obtained on the original information bits $\mathbf{u}$ so that final decisions may be made, D1 must also compute likelihood ratios on E1 information bits. For instance, D1 receives no samples directly from the channel; the only input to D1 is the extrinsic information produced by D2. The LLR $L(c_k)$ can be computed as [16],

$$L(c_k) = \max_{C^+}{}^{*} \left[\tilde{\alpha}_{k-1}(s') + \tilde{\gamma}_k(s', s) + \tilde{\beta}_k\right] - \max_{C^-}{}^{*} \left[\tilde{\alpha}_{k-1}(s') + \tilde{\gamma}_k(s', s) + \tilde{\beta}_k\right] \quad (36)$$

where C^+ is equal to the set of trellis transitions at time k for which $c_k = +1$ and similarly we define C^-. Here, the same notations are used for both decoders D1 and D2, α and β are the forward and backward recursion variables for both BCJR algorithms. The decoding order is D2 $\rightarrow$ D1 $\rightarrow$ D2 $\rightarrow$ D1 $\rightarrow \cdots$ The decoder D1 has only extrinsic information as input (the channel does not feed this decoder). Thus the branch transition metric for D1 is given as

$$\gamma_k(s', s) = u_k L_{21}^e(u_k)/2 + p_k L_{21}^e(pk)/2 \quad (37)$$

The detailed SC-SSB-FSK iterative decoding algorithm is presented in Algorithm 2 given in Appendix B. After executing the last iteration, the transition probability at D1 is calculated for the message binary bits only not for the encoded bits. Next, the final maximum log-likelihood function is obtained by,

$$L(u_k) = \max_{U^+}{}^{*} \left[\alpha_{k-1}^1(s') + \gamma_k(s', s) + \beta_k^1(s)\right] \max_{U^-}{}^{*} \left[\alpha_{k-1}^1(s') + \gamma_k(s', s) + \beta_k^1(s)\right]. \quad (38)$$

Finally, the detected message bits are given by,

$$\hat{u}_k = sign[L(u_k)] \quad (39)$$

V. SSB-FSK Parameter Analysis based on EXIT Chart

A. EXIT Analysis of SC-SSB-FSK

The EXIT chart analysis is a tool using the mutual information (MI) between the transmitted bits and the extrinsic LLRs to estimate the convergence threshold, which implicitly relies on a coset approach. The EXIT chart was first introduced in [19]. It is a common asymptotic tool used to analyze the convergence of iterative systems. It aims to calculate

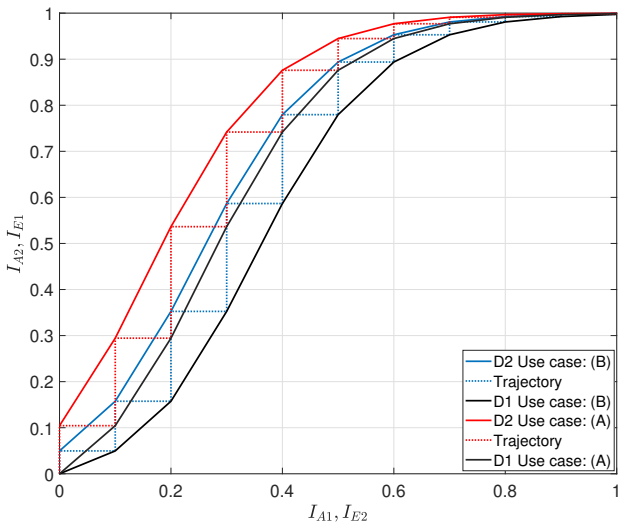

FIGURE 5. EXIT charts with a decoding trajectory for SC-SSB-FSK with use case (A) and (B) at $E_b/N_0 = 0$ dB

the input-output transfer function of a general SISO block. A general SISO block may have input LLRs from channel observations and some a priori LLRs. At the output, extrinsic information is computed for a given signal-to-noise ratio (SNR). Based on these inputs and outputs, the EXIT transfer function, denoted here by $\mathfrak{f}$, calculates the mutual information I_e between the transmitted bits and the external LLRs versus the mutual information I_a between the a priori LLRs and the corresponding bits, such that $I_a = \mathfrak{f}(I_e)$. This mutual information is directly related to LLR distributions. These LLRs can be assumed to be independent and identically distributed random variables for very large frames of data symbols. The mutual information between a binary random variable $x \in \{\pm 1\}$ and the corresponding LLRs is given by the following equation:

$$I(x, \text{LLR}) = \frac{1}{2} \sum_{x \in \pm 1} \int p(\text{llr}|x) \log_2 \left(\frac{2p(\text{llr}|x)}{p(\text{llr}|x=1) + p(\text{llr}|x=-1)} \right) d\text{llr} \quad (40)$$

Extrinsic information exchange is visualized as a decoding trajectory in EXIT Charts. Let I_{A1} and $I_{E2} = \mathbf{Z}_{12}(\mathbf{u})$ denote the prior and the MI for the CC. Similarly, let I_{A2} and I_{E1} denote the prior and extrinsic MI for the SSB-FSK modulator. I_{E1} and I_{E2} are found via separate Monte Carlo simulations of the two constituent codes for different values of E_b/N_0. $I_{E1} = T_1(I_{A2})$ and $I_{E2} = T_2(I_{A1})$, where T_1 and T_2 denote the EXIT functions of C_1 and C_2, respectively. The convergence threshold can be predicted by plotting the EXIT curves for C_1 and C_2 in a single diagram.

CPM introduces a strong constraint on the design of the concatenated code because it is part of it. It may then happen that a CPM scheme achieving higher capacity shows a poor

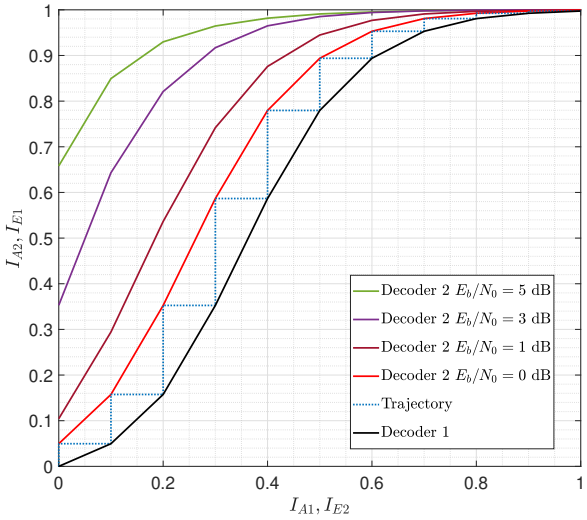

FIGURE 6. EXIT charts of the proposed iterative decoder of SC-SSB-FSK signal with use case (A) at $E_b/N_0 = 0, 1, 3,$ and 5 dB

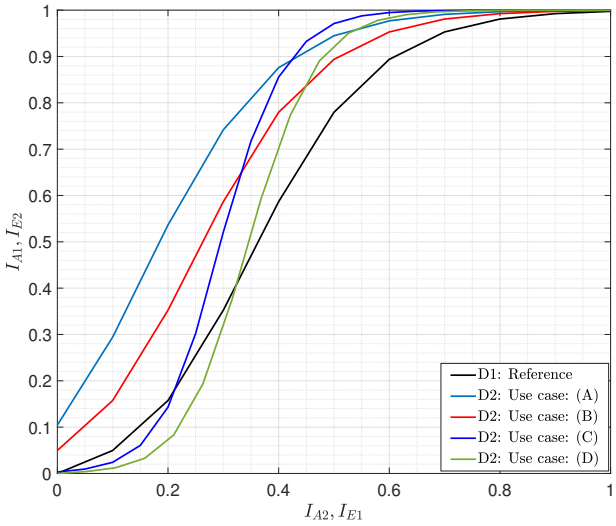

FIGURE 7. EXIT charts of the proposed iterative decoder of SC-SSB-FSK signal for the use cases (A, B, C, and D) at $E_b/N_0 = 0$ dB.

TABLE 1. Detail of the optimization parameters

	Parameter	Value or Range
Fixed Parameters	Modulation Order M	2
	Modulation Index h	1
	Pulse width w	0.8
	CC code rate	1/2
	CC generator polynomial	$[5, 7]_8$
Constraint Parameters	Pulse Shape	RC and Lorention
	ACI	0 to 5 dB
	Pulse length	$L \in [5, 9]$
	SNR	$E_b/n_0 \in [0, 1, 3, 5]$
	Number of iteration	$I_s \leq 10$
Target Parameters	Bandwidth occupancy η	99.9
	EXIT Tunnel width Ω	≥ 0

matching of the two EXIT curves when considered in a concatenated scenario, thus leading to poorer convergence thresholds than CPM schemes with lower capacity. It is not the case with linear modulations, where all degrees of freedom to design the channel code are available. The EXIT charts for the iterative decoder of SC-SSB-FSK signal are presented from Fig. 5 to Fig. 6 for SSB FSK parameter configurations (A) and (B) for different E_b/N_0.

Fig. 5 presents the EXIT chart plots with the transition trajectory of the mutual information of SC-SSB-FSK iterative decoder for use cases (A) and (B), respectively. In both figures, the number of iterations required by the iterative decoder for configuration (A) is equal to 7, and for configuration (B) is equal to 8. This can be explained by the increasing SSB-FSK pulse length L, which increases the number of possible states of the decoder structure, consequently increasing the complexity of the receiver. Thus, from Fig. 5 to 6, we can conclude that the convergence threshold of the iterative decoder depends on the trade-off of multiple parameters. Thus selecting the optimum parameter for the desired BER is a challenging task. In the next subsection, we present EXIT evolution-based optimization in the presence of ACI.

Next, we obtained the EXIT curve for the other two use cases, which gives the d^2_{min} close to the Pareto frontier with a non-integer modulation index, which are:

- Use case (C): $L = 2,\ h = 0.7,\ M = 2$ and $w = 0.9$,
- Use case (D): $L = 2,\ h = 0.6,\ M = 2$, and $w = 0.8$.

The d^2_{min} for (C) and (D) are 2.82 and 2.33, respectively. We have considered case B as the reference EXIT information curve. Fig. 7 clearly shows that the EXIT curve obtained for cases C and D is not better than the reference curve. This is an important observation that the Pareto optimum or d^2_{min} is not the only defining parameter for the performance of the concatenated SSB-FSK system, and we need to carry out the EXIT analysis in order to analyze the convergence of the performance. The next section shows the BER curve for cases (C) and (D), which also confirms that these cases, despite having d^2_{min} close to and higher than case (B), perform worse than case (B).

B. EXIT Optimization of SC-SSB-FSK in Presence of ACI

In this work, we consider the Pareto frontier SSB FSK parameters. In the previous subsection, we analyzed the EXIT chart for both Pareto frontier configurations (use cases A and B) of the SSB FSK signal, as well as the interesting configuration close to the Pareto optimal (use cases C and D). Thus, in this section, we present the optimum configuration

among all through the EXIT chart analysis in the presence of ACI. We consider a system where several users are frequency multiplexed, and the separation between two adjacent channels is F. Let $s_0(t)$ be the modulated CPM signal for the user of interest. The overall optimization parameter of a CPM scheme is presented in Table 1. We assume that two interferes employ the same modulation scheme as the user and are received with equal power in the adjacent channels so that the resulting overall signal at the receiver input is given by,

$$r(t) = \sqrt{P_s}s_0(t,a) + \sum_{k=-1;k\neq 0} \sqrt{P_I}s_k(t,a)e^{j2\pi kF} + n(t) \quad (41)$$

we do not consider the effect of the interference with $|k| > 1$, as we assume their impact is much less critical. The signal-to-noise ratio in decibels in the channel bandwidth F and the relative ACI level are

$$SNR_F = 10\log_{10}(P_s/FN_0) \quad \text{dB} \quad (42)$$

$$ACI = 10\log_{10}(2P_I/P_s) \quad \text{dB} \quad (43)$$

The choice of FT implicitly determines the rate R of the outer code, which is related as

$$R = \frac{\eta FT}{log_2 M} \quad (44)$$

We have considered $\Omega = I_{A2} - I_{A1}$ an EXIT tunnel width for the maximization. To converge the iterative decoder $\Omega \geq 0$, which creates the tunnel in the EXIT chart, and for negative $\Omega \leq 0$ the EXIT curve intersects each other, closing the iterative tunnel path of the EXIT chart. The EXIT chart analysis of the above-considered parameters is presented in the observation Table. 2. Table. 2, conclude that for a given optimization constraint for case (B), of the SSB-FSK parameter performed more optimistically even in the presence of ACI, as It can take only 6 iterative steps for $E_b/N_0 = 3$ dB and $ACI = 3$ dB. However, the RC pulse CPM signal converges at 5 iterative rounds. After careful observation of the Table. 2, we can conclude that the use case (A) of the iterative decoding of Lorentzian pulse-based SC SSB-FSK detection performs similarly to the iterative decoding of RC pulse-based SC CPM signal. Furthermore, use cases (C) and (D) are performing quite similarly from an iterative convergence point of view. Whereas the limitation of the EXIT chart is that it does not provide the BER performance information. Thus, in the next section, we thoroughly study the BER performance of iterative decoding of SC-SSB-FSK modulated signal.

VI. BER Simulation and Discussion

This section presents the BER performance analysis of iterative decoding of the SC-SSB-FSK system based on Sections III, IV, and V. The performance analysis is performed by considering many metrics and varying parameters, which are considered in Sections V-A and V-B. In the serial

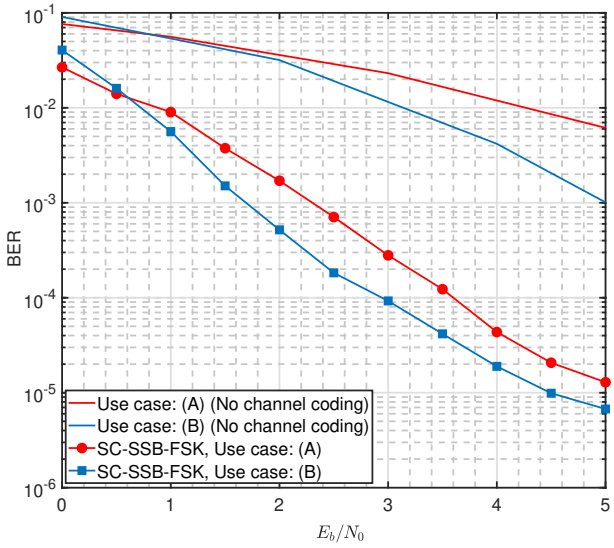

FIGURE 8. BER plots of SC SSB-FSK and its iterative decoding and BER of MAP detection of SSB-FSK without concatenated scheme for both SSB-FSK use cases (A) and (B).

concatenation scheme, the recursive convolutional encoder ($G = [1, 5/7]$) as the FEC code is concatenated with the novel SSB-FSK signal to improve the performance of the SSB-FSK-based communication system. However, the other configuration of FEC codes can be investigated to enhance the performance of the SC-SSB-FSK scheme, which is beyond the scope of this research and is kept as the future scope of this work. Therefore, in Fig. 8 to Fig. 13, we present the BER performance of the iterative decoding of SSB-FSK signal serially concatenated with CC ($G = [1, 5/7]$). The number of iterations considered is equal to 8 for all BER plots. Based on the EXIT chart analysis presented in the previous section, we fix the maximum number of iterations to 8, which is sufficient for all use cases (A), (B), (C) and (D) of SSB-FSK to converge.

In Fig. 8, the BER performance of the SC scheme of the SSB-FSK modulated signal and its iterative decoding is shown together with the performance of the SSB-FSK signal without the concatenation scheme. Fig. 8 clearly shows that the concatenated system greatly improves the BER performance because the concatenation scheme provides more robustness against noise. In addition, the channel code can increase the reliability of the transmission by correcting errors in the decoding result of the CPM signal. In Fig. 8 it can be seen that the BER $= 10^{-5}$ is achieved at $E_b/N_0 = 5$ dB with $L = 9$, $w = 0.8$, $h = 1$. Apart from this good performance of the presented SSB-FSK, the sideband power reduction may further enhance the performance of the iterative decoder. Thus the sideband power reduction based on [20] could be considered as the future scope of the presented research work.

This article has been accepted for publication in IEEE Open Journal of the Communications Society. This is the author's version which has not been fully edited and content may change prior to final publication. Citation information: DOI 10.1109/OJCOMS.2023.3310711

TABLE 2. Number of Required Iterations

ACI (dB)	Use case: (A) E_b/N_o (dB)				RC pulse ≈ (A) E_b/N_o (dB)				Use case: (B) E_b/N_o (dB)				RC pulse ≈ (B) E_b/N_o (dB)				Use case: (C) E_b/N_o (dB)				Use case: (D) E_b/N_o (dB)			
	0	1	3	5	0	1	3	5	0	1	3	5	0	1	3	5	0	1	3	5	0	1	3	5
0	7	7	6	6	8	7	6	6	8	8	7	7	8	7	6	5	10	8	7	7	9	8	7	6
1	8	6	5	5	8	7	5	6	8	8	6	7	8	7	5	5	10	9	7	6	9	8	6	6
3	8	6	8	8	8	7	5	7	8	8	6	6	8	7	5	5	10	9	6	7	9	8	6	6
Without ACI	7	6	4	3	7	6	5	5	7	6	5	4	7	6	5	6	9	8	7	7	10	9	8	7

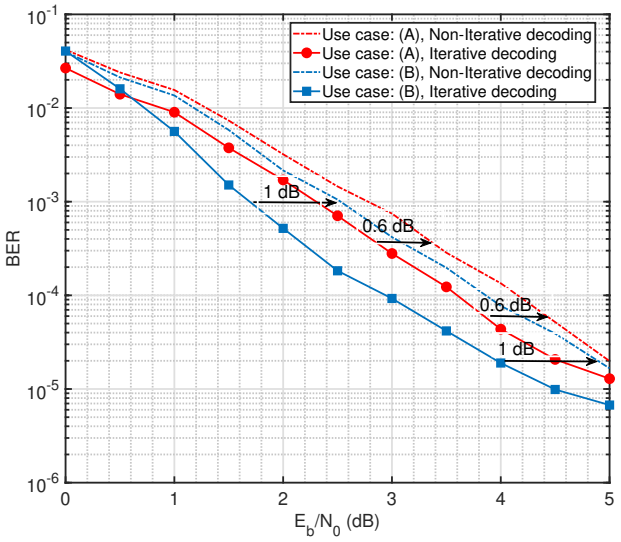

FIGURE 9. BER plots for iterative and Non-iterative decoding of SC SSB-FSK signal.

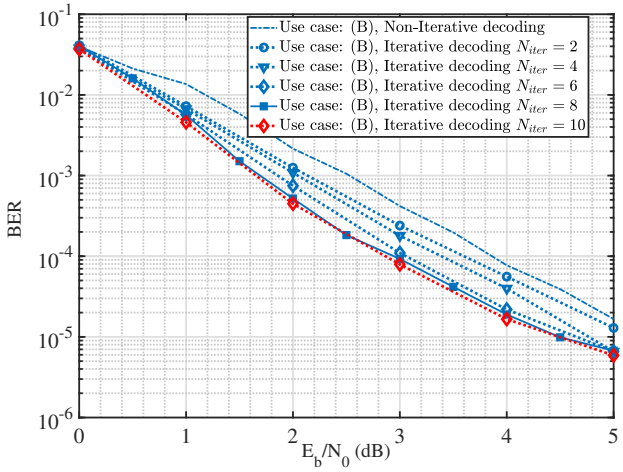

FIGURE 10. BER plots for iterative and Non-iterative decoding of SC SSB-FSK signal with the number of iterations.

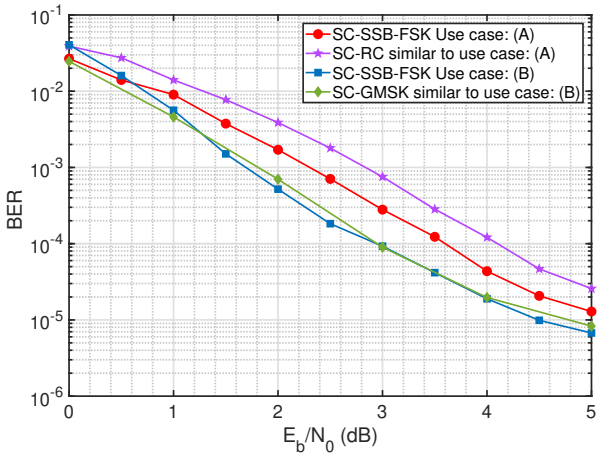

FIGURE 11. BER plots of SC-SSB-FSK, SC-RC-CPM, and SC-GMSK with iterative decoding.

In Fig. 9, we have compared the BER performance of non-iterative and iterative decoding of the SC-SSB-FSK modulated CPM signal. It is shown that the BER performance is improved significantly with iterative decoding compared to non-iterative decoding. For use case (A) (i.e., $L = 5,\ w = 0.8,\ h = 1$), around 0.6 dB of SNR gain is achieved, and for use case (B) (i.e., $L = 5,\ w = 0.8,\ h = 1$), around 1 dB of SNR gain is achieved. Therefore, depending on the priority of the designer among all performance metrics, iterative decoding can be or not adopted. For instance, if low-complexity detection is the absolute priority of the designer, then iterative schemes are not needed. In Fig. 10, we have presented the BER performance of iterative decoding with various iterations ($N_{iter} = [2, 4, 6, 8, 10]$) for the Use case (B). It is clearly shown that with the increased number of N_{iter}, the BER performance of iterative decoding is increasing. we have demonstrated that the feasibility of designing the optimal number of iterations using the EXIT technique, i.e. $N_{iter} = 8$ gives the optimum BER performance also, $N_{iter} = 10$ does not give any significant performance enhancement (which is coherent with the result already predicted by the EXIT technique).

In Fig. 11, we have compared the BER performance SC SSB-FSK with the state-of-art RC and GMSK-based SC-CPM signal. It is illustrated that the BER performance is optimum throughout compared to the RC pulse SC-CPM. This optimum performance is expected, as we have used the Pareto frontier, which has better $d^2_{\min}$ configuration. This Pareto front comparison of SSB-FSK and RC is illustrated in

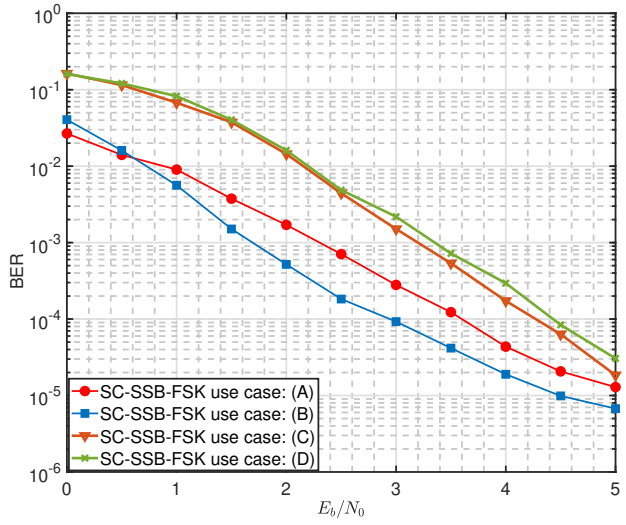

FIGURE 12. BER plots for the use case (A, B, C, and D).

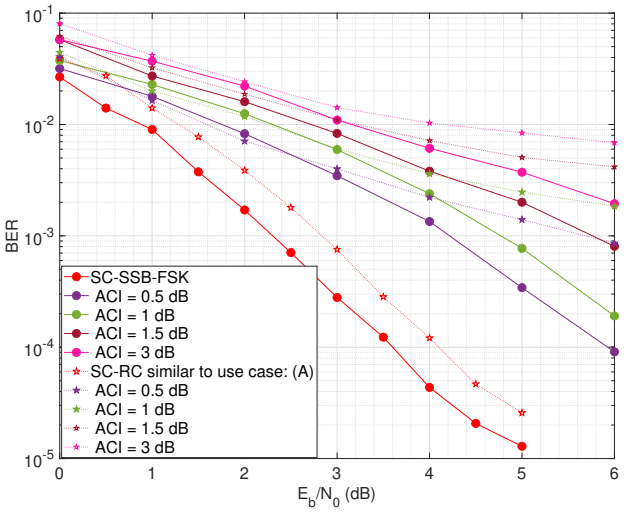

FIGURE 13. BER plots of SC-SSB-FSK for the use case (A) compared to SC-RC CPM in the presence of various ACI amounts.

Figure 3.11 of [21]. Further, it is obtained that the proposed algorithm performance is almost similar to and better than the state-of-art GMSK in high SNR values in use case B. It is clearly obtained from the figure that GMSK performs better than the proposed algorithm at low SNR, i.e. $E_b/N_0 = 0$ to 1 dB, and performs equally similar at mid-SNR, i.e. $E_b/N_0 =$ 3 to 4 dB. However, the proposed algorithm performs better at $E_b/N_0 = 1.5$ to 2.5 dB and $E_b/N_0 \geq 4$ dB.

In Fig. 12, BER curves are plotted for all use cases. In all scenarios, we have considered $M = 2$ to reduce the computational complexity of the receiver. It has been observed that the (C) and (D) cases underperform even though they have d^2_{min} higher than (B). We recall here that use cases (C) and (D) have non-integer modulation indices. From this surprising observation, we can make an insightful conclusion, which is d^2_{min} can not be the unique metric to classify SSB-FSK schemes when they are used in a concatenated manner. Besides, the possible reason for the underperformance of the SC scheme in the (C) and (D) cases is that $L = 2$ provides less coding gain making the system more vulnerable to noise. The BER plots of the iterative decoder for both SC-SSB-FSK and SC-RC CPM in the presence of ACI are presented in Fig. 13. Fig. 13 depicts that with the increase in the ACI value, the BER performance decreases significantly as the ACI increases the interference in the received signal for both CPM schemes (SSB-FSK or RC-based). However, Fig. 13 also illustrates that the performance of SC-SSB-FSK is always better compared to the RC-based CPM modulation since the received signal of SSB-FSK is affected by less interference (only from one side adjacent channel) due to its strong SSB property whereas RC-based CPM signal has interference from both side adjacent channels. This is a relevant reason to prefer SSB-FSK based systems to familiar CPM based systems, which are generating all of them double-sided spectrum signals (more vulnerable to interference).

VII. Conclusion

In this paper, an SC-SSB-FSK with a CC and its iterative decoding based on PAM decomposition is presented. Furthermore, using this system implementation, an extensive MATLAB-based simulation is carried out to analyze the feasibility of the SC schemes using this new SSB-FSK CPM family. To do so, an EXIT-chart analysis is used to obtain the convergence capabilities of the iterative decoder. The reported Pareto frontier parameters of SSB-FSK as well as other interesting configurations close to the Pareto frontier, are used to analyze the EXIT chart performance. The performance of the iterative decoder in the presence of ACI is analyzed. The optimization results are given in terms of the minimum number of iterations required to converge under given environmental conditions, assuming a fixed amount of ACI. We have illustrated the BER performance of the proposed iterative decoder on the retained SC-SSB-FSK configurations resulting from the EXIT-based optimization. The BER analysis of SC-SSB-FSK is compared to the RC-CPM signal, and it has been shown that the proposed technique outperforms state-of-the-art serially concatenated CPM-based systems. One of the most important contributions of this paper is the implementation of the iterative decoding of the SC-SSB-FSK signal based on the PAM decomposition and the performance through simulation study to demonstrate the feasibility of the SSB-FSK signal in a practical scenario. To design competitive SC-SSB-FSK systems, two particular configurations, i.e., use cases (A) and (B), have been retained since they combine several advantages: good iterative convergence, reasonable complexity, synchronization advantage (having integer modulation index), and finally robust transmission in the presence of ACI

since they are generating pure SSB spectrum (also resulting from this integer modulation index).

REFERENCES

[1] H. Farès, D. C. Glattli, Y. Louët, J. Palicot, C. Moy, and P. Roulleau, "From quantum physics to digital communication: Single sideband continuous phase modulation," *Comptes Rendus Physique*, vol. 19, no. 1-2, pp. 54–63, 2018.

[2] J. Dubois, T. Jullien, F. Portier, P. Roche, A. Cavanna, Y. Jin, W. Wegscheider, P. Roulleau, and D. Glattli, "Minimal-excitation states for electron quantum optics using levitons," *Nature*, vol. 502, no. 7473, pp. 659–663, 2013.

[3] T. Jullien, P. Roulleau, B. Roche, A. Cavanna, Y. Jin, and D. Glattli, "Quantum tomography of an electron," *Nature*, vol. 514, no. 7524, p. 603, 2014.

[4] H. Farès, C. Glattli, Y. Louët, C. Moy, J. Palicot, and P. Roulleau, "New binary single side band CPM," in *2017 24th International Conference on Telecommunications (ICT)*, pp. 1–5, 2017.

[5] K. Kassan, H. Farès, D. C. Glattli, and Y. Louët, "Simplified receivers for generic binary single side band CPM using PAM decomposition," *IEEE Access*, vol. 9, pp. 115962–115971, 2021.

[6] G. K. Kaleh, "Simple Coherent Receivers for Partial Response Continuous Phase Modulation," *IEEE Journal on Selected Areas in Communications*, vol. 7, no. 9, pp. 1427–1436, 1989.

[7] K. Kassan, H. Farès, D. C. Glattli, and Y. Louët, "Performance vs. spectral properties for single-sideband continuous phase modulation," *IEEE Transactions on Communications*, vol. 69, no. 7, pp. 4402–4416, 2021.

[8] P. Moqvist and T. M. Aulin, "Serially concatenated continuous phase modulation with iterative decoding," *IEEE Transactions on Communications*, vol. 49, no. 11, pp. 1901–1915, 2001.

[9] N. Noels, M. Moeneclaey, F. Simoens, and D. Delaruelle, "A low-complexity iterative phase noise tracker for bit-interleaved coded CPM signals in AWGN," *IEEE transactions on signal processing*, vol. 59, no. 9, pp. 4271–4285, 2011.

[10] M. Xiao and T. M. Aulin, "Serially concatenated continuous phase modulation with symbol interleavers: performance, properties and design principles," in *IEEE Global Telecommunications Conference, 2004. GLOBECOM'04.*, vol. 1, pp. 179–183, IEEE, 2004.

[11] L. S. Levitov, H. Lee, and G. B. Lesovik, "Electron counting statistics and coherent states of electric current," *Journal of Mathematical Physics*, vol. 37, no. 10, pp. 4845–4866, 1996.

[12] H. Farès, D. C. Glattli, Y. Louet, J. Palicot, P. Roulleau, and C. Moy, "Power spectrum density of single side band CPM using lorenztian frequency pulses," *IEEE Wireless Communications Letters*, vol. 6, no. 6, pp. 786–789, 2017.

[13] X. Huang and Y. Li, "The PAM decomposition of CPM signals with integer modulation index," *IEEE transactions on communications*, vol. 51, no. 4, pp. 543–546, 2003.

[14] P. Laurent, "Exact and approximate construction of digital phase modulations by superposition of amplitude modulated pulses (amp)," *IEEE transactions on communications*, vol. 34, no. 2, pp. 150–160, 1986.

[15] M. Messai, K. Amis, and F. Guilloud, "On the optimization of a PSP-based CPM detection," *IEEE transactions on wireless communications*, vol. 15, no. 3, pp. 2144–2154, 2015.

[16] W. Ryan and S. Lin, *Channel codes: classical and modern*. Cambridge university press, 2009.

[17] J. B. Anderson, T. Aulin, and C.-E. Sundberg, *Digital phase modulation*. Springer Science & Business Media, 2013.

[18] Z. Xu and Q. Wang, "Autocorrelation Function of Full-Response CPM Signals and Its Application to Synchronization," *IEEE Access*, vol. 7, pp. 133781–133786, 2019.

[19] S. Ten Brink, "Convergence behavior of iteratively decoded parallel concatenated codes," *IEEE transactions on communications*, vol. 49, no. 10, pp. 1727–1737, 2001.

[20] Z. Liu, Y. L. Guan, and C.-C. Chui, "Cpm training waveforms with autocorrelation sidelobes close to zero," *IEEE Transactions on Vehicular Technology*, vol. 67, no. 11, pp. 11269–11273, 2018.

[21] K. Kassan, *Performance of a new single sideband (SSB) continuous phase modulation (CPM)*. PhD thesis, CentraleSupelec, 2021.

Appendix

A. BCJR Detection of SSB FSK modulated signal

Algorithm 1 :

1: Initialize the $\alpha_0(s)$ and $\beta_N(s)$ based on (34) and (35), respectively.
2: Compute $\gamma(s', s)$ = based on eq (27) of [5].
3: **for** $i = 1 \text{to} N-1$ **do**
4: Compute $\alpha_i(s)$ for all s by using recursion $\alpha_i(s) = \max^*_{s'}[\alpha_{i-1}(s') + \gamma_i(s', s)]$
5: **end for**
6: **for** $i = N$ to 2 **do**
7: Compute $\beta_i(s)$ for all s by using recursion $\beta_{i-1}(s') = \max^*_{s}[\beta_i(s') + \gamma_i(s', s)]$
8: **end for**
9: **for** $i = N$ to 2 **do**
10: Compute $L(\hat{a}_i)$ using (33)
11: Compute hard decisions via $\hat{a}_i = \text{sign}[L(\hat{a}_i)]$
12: **end for**

B. The SC-SSB-FSK Iterative Decoder

Algorithm 2 :

D1:

Initialize the $\alpha_0^1(s)$ and $\beta_K^1(s)$ as:

$$\alpha_0^1(s) = \beta_K^1(s) = \begin{cases} 0, & s = 0, \\ -\infty & s \neq 0 \end{cases} \tag{45}$$

D2:.

Initialize the $\alpha_0^2(s)$ and $\beta^2(s)$ as:

$$\alpha_0^2(s) = \begin{cases} 0, & s = 0, \\ -\infty & s \neq 0 \end{cases} \text{ and, } \beta^2(s) = \alpha_0^2(s)$$

The n^{th} iteration

for $k = 1$ to $2K$ **do**

get $y_k = [y_k^v, y_k^q]$

Compute $\gamma_k(s', s)\ \forall\ s' \to s$,

$$\gamma_k(s', s) = v_k L_{12}^e(v_k)/2 + v_k y_k^v/\sigma^2 + q_k y_k^q/\sigma^2$$

Compute $\alpha_k^2(s)$ by,

$$\alpha_k^2(s) = \max_{s'}{}^{*} \left[\alpha_{k-1}^2(s') + \gamma_k(s', s)\right]$$

end for

for $k = 2K$ to 2 **do**

Compute $\beta_{k-1}^2(s')$ by,

$$\beta_{k-1}^2(s') = \max_{s} * \left[\beta_k^2(s) + \gamma_k(s', s)\right]$$

end for

for $k = 1$ to $2K$ **do**

Compute $L_{12}^e(v_k)$ using

$$L_{12}^e(v_k) = \max_{V^+}{}^{*} \left[\alpha_{k-1}^2(s') + \gamma_k(s', s) + \beta_k^2(s)\right] \max_{V^-}{}^{*} \left[\alpha_{k-1}^2(s') + \gamma_k(s', s) + \beta_k^2(s)\right] - L_{12}^e$$

end for

D1:

for $k = 1$ to K **do**

Compute $\gamma_k(s', s)$ by using (37)

Compute α_k^1 for all s by

$$\alpha_k^1(s) = \max_{s'}{}^{*} \left[\alpha_{k-1}^1(s') + \gamma_k(s', s)\right]$$

end for

for $k = K$ to 2 **do**

Compute $\beta_{k-1}^1(s')$ by,

$$\beta_{k-1}^1(s') = \max_{s} * \left[\beta_k^1(s) + \gamma_k(s', s)\right]$$

end for

for $k = 1$ to K **do**

Compute $L_{12}^e(u_k)$ by,

$$\begin{aligned} L_{12}^e(u_k) = &\max_{U^+}{}^{*} \left[\alpha_{k-1}^1(s') + \gamma_k(s', s) + \beta_k^1(s)\right] \\ &- \max_{U^-}{}^{*} \left[\alpha_{k-1}^1(s') + \gamma_k(s', s) + \beta_k^1(s)\right] \\ &- L_{21}^e(c_{2k-1}^1) \\ = &\max_{U^+}{}^{*} \left[\alpha_{k-1}^1(s') + p_k L_{21}^e(p_k)/2 + \beta_k^1(s)\right] \\ &\max_{U^-}{}^{*} \left[\alpha_{k-1}^1(s') + p_k L_{21}^e(p_k)/2 + \beta_k^1(s)\right] \end{aligned}$$

Compute $L_{12}^e(p_k)$ by,

$$\begin{aligned} L_{12}^e(p_k) = &\max_{U^+}{}^{*} \left[\alpha_{k-1}^1(s') + u_k L_{21}^e(u_k)/2 + \beta_k^1(s)\right] \\ &- \max_{U^-}{}^{*} \left[\alpha_{k-1}^1(s') + u_k L_{21}^e(u_k)/2 + \beta_k^1(s)\right] \end{aligned}$$

end for

Abhishek Kumar received a bachelor's in electronics and telecommunication engineering from the Institution of Electronics and Telecommunication Engineering (IETE) New Delhi, India in 2011, master's degree in digital communication from the University School of Information Technology GGSIPU New Delhi, India in 2014, and the Ph.D. degree in electronics and communication engineering from National Institute of Technology Patna, India in 2021. He is currently a postdoc scholar at CentraleSupélec of Rennes, Universite Paris Saclay France. He is a member of SIGNAL research group of the CNRS Institute of Electronics and Digital Technologies (IETR), Rennes Laboratory. He is a member of the IEEE, IETE, and URSI. His research interests include the area of communication theory, including nonlinear modulations, iterative decoding algorithms, cognitive radio, and the PHY layer of 5G and nextG communication systems. He is the recipient of a young scientist award at the IEEE URSI-GASS symposium in Rome, Italy, in 2020.

Haïfa Farès received the bachelor's and M.Sc. degrees in telecommunication engineering from the Higher School of Communications of Tunis (Sup'Com), in 2007 and 2008, respectively, and the Ph.D. degree in digital communications from IMT-Atlantique, France, in 2011. She is currently an Associate Professor at CentraleSupélec of Rennes. She is a member of SIGNAL research group of the CNRS Institute of Electronics and Digital Technologies (IETR), Rennes Laboratory. Her research interests include the area of communication theory, including nonlinear modulations, green communications, iterative decoding algorithms, and non-orthogonal multiple access.

Yves Louët received the Ph.D. degree in digital communications from Rennes University, France, in 2000, and the Habilitation degree (HDR; research) from Rennes University, in 2010. The topic of his Ph.D. thesis regarded peak to average power reduction in OFDM modulation with channel coding. He was a Research Engineer with SIRADEL Company, Rennes, in 2000, and was involved in channel propagation modeling for cell planning. He was also involved in French collaborative research projects, including COMMINDOR, ERASME, and ERMITAGES about channel modeling in many frequency bands, especially, 60 and five GHz for further telecommunication systems.

In 2002, he joined Supélec as an Associate Professor. His teaching and research activities were in line with signal processing and digital communications applied to software and cognitive radio systems. He was involved in many collaborative European projects, including FP7E2R, CELTIC B21C, CELTIC SHARING, NoE Newcom, COST, and French projects, including ANR PROFIL, ANR INFOP,WONG5, FUI AMBRUN, APOGEES, TEPN, and WINOCOD. His research contribution is mainly focused on new waveforms design for green cognitive radio and energy efficiency enhancement. In 2010, he became a Full Professor with Supélec and later CentraleSupélec. He is the Head of the Signal and Communication department (including two research teams, i.e., ASIC and SIGNAL), belonging to the CNRS Institute of Electronics and Digital Technologies (IETR), Rennes Laboratory. He is also President of the URSI Commission C.